

SUPPLEMENTAL MATERIAL

Li, W., et al., 2020, Redox state of southern Tibetan upper mantle and ultrapotassic magmas: *Geology*, v. 48, <https://doi.org/10.1130/G47411.1>

PETROGRAPHIC FEATURES OF MANTLE XENOLITHS

Mantle xenoliths occurred in Sailipu trachyandesites mainly consist of lherzolite. They display porphyroclastic texture, comprising larger grains (0.05–1 mm) of ~55% olivine, ~25% orthopyroxene, ~15% clinopyroxene, <2% phlogopite, and a few fine-grained (<50 μm) spinel and apatite (Fig. S5A). Olivine and orthopyroxene (100–500 μm) are mainly euhedral to subhedral with curvilinear boundaries (Fig. S5A). Clinopyroxene is smaller in size (30–100 μm ; Fig. S5A), and often shows embayed texture filled by orthopyroxene (Fig. S5B), indicating disequilibrium between the two pyroxene types. Anhedral phlogopite mainly occurs in the interstices between large olivine and orthopyroxene (Fig. S5A). Spinel is small in size (1–20 μm) with vermicular texture, and frequently occur as inclusions in large olivine, orthopyroxene, and clinopyroxene (Figs. S5A–S5C).

METHODS SUMMARY

Analytical methods

Electron microprobe analysis

Olivine, spinel, orthopyroxene and clinopyroxene in harzburgite xenoliths were analyzed by electron microprobe analyses (EMPA) using a JEOL JXA-8230 Superprobe at the Institute of Mineral Resources, Chinese Academy of Geological Sciences. The microprobe was operated at an accelerating voltage of 15 kV, 20 nA probe current, and a beam diameter of 1 to 5 μm . Natural minerals and synthetic oxides were used as standards. Matrix corrections were performed using the ZAF correction program supplied by the instrument manufacturer. The limit of detection for major elements fall within the range of 77–244 ppm, the accuracy is within 5%. Analyzed major element compositions of minerals are reported in Tables S1–S3, which will be used in the following temperature, pressure and oxygen fugacity ($f\text{O}_2$) calculation based on different thermometers, barometers and oxybarometers (see section of Calculation methods).

Trace elements analysis by LA-ICP-MS

Trace element concentrations in olivine phenocrysts of ultrapotassic volcanic rocks were analyzed by LA-ICP-MS at University of Tasmania. This instrumentation comprises a New Wave Research UP213 Nd-YAG (213 nm) laser coupled to an Agilent 4500 quadrupole mass spectrometer. Analyses were performed by ablating 30–60 μm diameter spots at a rate of 10 shots/s. Data reduction was undertaken according to standard methods (Longerich et al., 1996) using the NIST612 glass as a primary reference material and the USGS BCR2 g glass as a secondary reference material. Vanadium content in olivines will be used to calculate magmatic $f\text{O}_2$ through the partitioning of vanadium between olivine phenocryst and silicate melt (see section of Calculation methods). Analyzed results and error

are reported in [Tables S3 and S6](#).

Laser Raman Spectroscopy

Laser Raman Spectroscopy was performed to obtain compositions of gas bubbles in mineral and melt inclusions ([Fig. S3](#)) at room temperature in University of Geneva. Raman spectra were typically obtained after 2 accumulations with an integration time of 50s and a spectral band pass of about 5 cm⁻¹. Raman spectra have been calibrated using Ar + plasma and neon emission lines and include various analytical instruments and parameters such as: Olympus BX40 microscope with motorized stage (X, Y, Z) using reflected and transmitted lights, 100x magnification, camera and green laser. The spectral images were processed with the Labspec software.

Wet chemistry

Ultrapotassic volcanic rocks were trimmed to remove surfaces, cleaned with deionized water, crushed, and powdered in an agate mill. Wet chemical analyses were carried out at Activation Laboratories Ltd. Sample powder was mixed with a flux of lithium metaborate and tetraborate, and fused in an induction furnace. The molten mixture was poured into a 5% nitric acid solution containing an internal standard, and mixed continuously until completely dissolved (~30 min.). More detailed methods are available from Actlabs (<http://www.actlabs.com>). Major and selected trace elements (e.g., Ba, Sr, and V) were analyzed by ICP–MS (Thermo Jarrell-Ash ENVIRO II ICP or Varian Vista 735 ICP), with reference materials NIST694, DNC1, GBW07113, NIST1613b, SY4, and BIR1a being analyzed in parallel. Analytical precisions were 1%–2%. Accuracy for major elements, as determined by reproducibility of standard and duplicate analyses, was typically within ±5% (≤±3% for SiO₂ and Al₂O₃). Trace element analyses involved digestion of sample powder in aqua regia with reference materials for the metals of interest. Samples and standards were analyzed by ICP–MS (Perkin Elmer Sciex 9000). Accuracy for trace elements was within ±10%. Analyzed data are listed in [Table S5](#).

Calculation methods

Thermometers & Barometers

Temperature and pressure of lherzolite xenoliths are calculated using the sensitive single clinopyroxene barometer ([Nimis and Taylor, 2000](#)) and thermometer (equation 32d of [Putirka, 2008](#)) which were shown to provide high reliability for many different kinds of mantle peridotites (e.g., [Nimis and Grütter, 2010](#)), expressed as:

$$P(kbar) = T(K)/126.9 \times \ln(a_{CaCrTs}^{Cpx}) - 15.483 \times \ln(Cr\#^{Cpx}/T(K)) + T(K)/71.38 + 107.8 \quad (1)$$

where $T(K)$ is temperature in Kelvin, and $P(kbar)$ is pressure in kbar. $a_{CaCrTs}^{Cpx} = Cr - 0.81 \times Cr\#^{Cpx} \times (Na+K)$ and $Cr\#^{Cpx} = Cr/(Cr+Al)$, with cations calculated on the basis of 6 oxygens. Standard error of pressure is ±3.1 kbar.

$$T(^{\circ}C) = (93100 + 544 \times P(kbar)) / (61.1 + 36.6 \times X_{Ti}^{Cpx} + 10.9 \times X_{Fe}^{Cpx} - 0.95 \times (X_{Al}^{Cpx} + X_{Cr}^{Cpx} - X_{Na}^{Cpx} - X_K^{Cpx})) + 0.395 \times (\ln(a_{En}^{Cpx}))^2 - 273.15 \quad (2)$$

where X_i^{cpx} represents cation fraction of i on the basis of 6 oxygens. a_{En}^{cpx} is the activity of enstatite in clinopyroxene, $a_{En}^{cpx} = (1 - X_{Ca}^{cpx} - X_{Na}^{cpx} - X_K^{cpx}) \times (1 - 0.5 \times (X_{Al}^{cpx} + X_{Cr}^{cpx} + X_{Na}^{cpx} + X_K^{cpx}))$. Standard error of temperature is ± 58 °C. Each pair of calculated temperature and pressure by single clinopyroxene grain will serve the fO_2 calculation (following equation 5).

For ultrapotassic volcanic rocks, the clinopyroxene–liquid thermobarometers (Putirka et al., 2003) are used to calculate temperature and pressure:

$$P(kbar) = -88.3 + 0.00282 \times T(K) \times \ln(Jd^{cpx} / (Na^{liquid} \times Al^{liquid} \times (Si^{liquid})^2)) + 0.0219 \times T(K) - 25.1 \times \ln(Ca^{liquid} \times Si^{liquid}) + 7.03 \times Mg^{liquid} + 12.4 \times \ln(Ca^{liquid}) \quad (3)$$

$$T(^{\circ}C) = 10000 / (4.6 - 0.437 \times \ln(Jd^{cpx} \times Ca^{liquid} \times Fm^{liquid} / (DiHd^{cpx} \times Na^{liquid} \times Al^{liquid}))) - 0.654 \times \ln(Mg^{liquid}) - 0.326 \times \ln(Na^{liquid}) - 0.00632 \times P(kbar) - 0.92 \times \ln(Si^{liquid}) + 0.274 \times \ln(Jd^{cpx}) - 273.15 \quad (4)$$

where pyroxene cations are calculated on the basis of 6 oxygens. Jd^{cpx} is the mole fraction of jadeite in clinopyroxene, and Jd is the lesser of Na or ^{VI}Al ; remaining Al is used to form CaTs. $DiHd^{cpx}$ is the mole fraction of diopside + hedenbergite in clinopyroxene, calculated as the fraction of Ca remaining after forming CaTs ($= ^{VI}Al - Jd$), $CaTiAl_2O_6$ ($= (^{IV}Al - CaTs)/2$), and $CaCr_2SiO_6$ ($= Cr/2$). Terms such as Al^{liquid} refer to the cation fraction of $AlO_{1.5}$ in the liquid, Fm^{liquid} is the sum $FeO^{liquid} + MgO^{liquid}$, and $Mg^{liquid} = MgO^{liquid} / (MgO^{liquid} + FeO^{liquid})$. Standard errors of pressure and temperature are ± 1.7 kbar and ± 33 K, respectively. All calculated temperature and pressure results are listed in Table S2. In this study, calculated temperature and pressure results through equation 3 and 4 will be averaged, then averaged values will be used to calculate ΔFMQ values through the following equation 6.

Results calculated by other thermometers (e.g., Helz and Thornber, 1987; Ballhaus et al., 1991; Sisson and Grove, 1993; Putirka, 2008) were also used for comparison and provided in Tables S1 and S2.

Oxybarometers

The oxybarometer of Ballhaus et al. (1991) was used to calculate the fO_2 of lherzolite xenoliths. It is expressed as:

$$\Delta FMQ = 0.27 + 2505/T(K) - 400 \times P(GPa)/T(K) - 6 \times \log(X_{Fe}^{ol}) - 3200 \times (1 - X_{Fe}^{ol})^2/T(K) + 2 \times \log(X_{Fe}^{sp}) + 4 \times \log(X_{Fe}^{sp}) + 2630 \times (X_{Al}^{sp})^2/T(K) \quad (5)$$

where ΔFMQ is the deviation of $\log fO_2$ from the fayalite-magnetite-quartz (FMQ) buffer (O'Neill 1987). X_{Fe}^{sp} and X_{Al}^{sp} represent the $Fe^{3+}/\Sigma R^{3+}$ and $Al/\Sigma R^{3+}$ ratio in spinel, X_{Fe}^{ol} and X_{Fe}^{sp} are the $Fe^{2+}/(Fe^{2+} + Mg)$ ratios in olivine and spinel, respectively. All used olivine–spinel pairs were selected in core areas of large olivine grains (e.g., Fig. S5C). Because of the lack of spinel in trachyandesite and trachyte, this oxybarometer thus does not apply to ultrapotassic volcanic rocks.

The Fe^{3+} and Fe^{2+} cations of spinels were calculated by normalizing spinel cation proportions to 3 total cations, treating all Fe as Fe^{2+} , and adjusting the Fe^{3+}/Fe^{2+} cation ratios to balance the charge deficiency or excess to 4 oxygens per 3 cations (Stormer, 1983). Then a Cr#-based correction to these calculated Fe^{3+}/Fe^{2+} cation ratios was applied. At the beginning and end of each electron microprobe

session, we measured calibration spinel standards with $\text{Fe}^{3+}/\text{Fe}^{2+}$ ratios previously characterized by Mössbauer spectroscopy. After calculating $\Delta\text{Fe}^{3+}/\Sigma\text{Fe}^{\text{Möss-EMPA}}$ and Cr\# ($=\text{Cr}/(\text{Cr}+\text{Al})$) for each calibration spinel measurement, the slope (A) and intercept (B) of the best fit line can be determined (Wood and Virgo, 1989; Birner et al., 2016): $\Delta\text{Fe}^{3+}/\Sigma\text{Fe}^{\text{Möss-EMPA}} = A \times \text{Cr\#} + B$. For comparison, the oxybarometer of Wood et al. (1990) was also used to calculate the $f\text{O}_2$. All calculated $f\text{O}_2$ values of lherzolite xenoliths are listed in Table S1.

The $f\text{O}_2$ values of ultrapotassic volcanic rocks was calculated through a new oxybarometer (i.e., the $D_V^{\text{ol/melt}}$ oxybarometer) calibrated by Mallmann and O'Neill (2013), based on the partitioning of vanadium (V) between olivine phenocryst and silicate melt:

$$\Delta FMQ = -7.7 - (\log D_V^{\text{ol/melt}}) / 0.2639 - (822 - 3328 \times (1 - Mg_{\#}^{\text{ol}})^2 + 5326 \times X_{\text{K0.5}}^{\text{melt}} + 746 \times (X_{\text{CaO}}^{\text{melt}} + X_{\text{NaO0.5}}^{\text{melt}}) - 3254 \times (X_{\text{SiO2}}^{\text{melt}} + X_{\text{AlO1.5}}^{\text{melt}})) / (0.2639 \times T(K)) \quad (6)$$

where $Mg_{\#}^{\text{ol}} = \text{Mg}/(\text{Mg}+\text{Fe})$, X_i^{melt} is mole fraction of each element ($i = \text{K, Ca, Na, Si, Al}$) in the melt on the single-cation basis (Tuff and O'Neill, 2010). Calculated $f\text{O}_2$ values of ultrapotassic volcanic rocks are listed in Table S3.

Systemic error estimations of all calculations of temperature, pressure and $f\text{O}_2$ have been made by error propagation, considering both error from analyzed data and calibrations of different thermometers, barometers, and oxybarometers. Estimated errors are listed in Tables S1 and S3, and shown as error bars in Fig. 2.

REFERENCES CITED

- Ballhaus, C., Berry, R. F., and Green, D. H., 1991, High pressure experimental calibration of the olivine-orthopyroxene-spinel oxygen geobarometer: implications for the oxidation state of the upper mantle: Contributions to Mineralogy and Petrology, 107(1), 27-40, <https://doi.org/10.1007/BF00311183>
- Birner, S. K., Warren, J. M., Cottrell, E., and Davis, F. A., 2016, Hydrothermal alteration of seafloor peridotites does not influence oxygen fugacity recorded by spinel oxybarometry: Geology, 44(7), 535-538, <https://doi.org/10.1130/G38113.1>
- Helz, R. T., and Thornber, C. R., 1987, Geothermometry of Kilauea Iki lava lake, Hawaii: Bulletin of volcanology, 49(5), 651-668, <https://doi.org/10.1007/BF01080357>
- Longerich, H. P., Jackson, S. E., and Gunther, D., 1996, Laser ablation inductively coupled plasma mass spectrometric transient signal data acquisition and analyte concentration calculation: Journal of Analytical Atomic Spectrometry 11, 899-904.
- Mallmann, G., and O'Neill, H. S. C., 2013, Calibration of an empirical thermometer and oxybarometer based on the partitioning of Sc, Y and V between olivine and silicate melt: Journal of Petrology, 54(5), 933-949, <https://doi.org/10.1093/petrology/egt001>
- Nimis, P., and Grütter, H., 2010, Internally consistent geothermometers for garnet peridotites and pyroxenites: Contributions to Mineralogy and Petrology, 159(3), 411-427, <https://doi.org/10.1007/s00410-009-0455-9>
- Nimis P. and Taylor W. R., 2000, Single clinopyroxene thermobarometry for garnet peridotites. Part 1 Calibration and testing of a Cr-in-cpx barometer and an enstatite-in-cpx thermometer:

- Contributions to Mineralogy and Petrology, 139:541-554, <https://doi.org/10.1007/s004100000156>
- O'Neill, H. S., 1987, Quartz-fayalite-iron and quartz-fayalite-magnetite equilibria and the free energy of formation of fayalite (Fe_2SiO_4) and magnetite (Fe_3O_4). *American Mineralogist*, 72(1-2), 67-75.
- Putirka, K. D., 2008, Thermometers and barometers for volcanic systems: Reviews in mineralogy and geochemistry, 69(1), 61-120, <https://doi.org/10.2138/rmg.2008.69.3>
- Putirka, K. D., Mikaelian, H., Ryerson, F., and Shaw, H., 2003, New clinopyroxene-liquid thermobarometers for mafic, evolved, and volatile-bearing lava compositions, with applications to lavas from Tibet and the Snake River Plain, Idaho: *American Mineralogist*, 88(10), 1542-1554, <https://doi.org/10.2138/am-2003-1017>
- Sisson, T. W., and Grove, T. L., 1993, Experimental investigations of the role of H_2O in calc-alkaline differentiation and subduction zone magmatism: *Contributions to mineralogy and petrology*, 113(2), 143-166, <https://doi.org/10.1007/BF00283225>
- Stormer, J. C., 1983, The effects of recalculation on estimates of temperature and oxygen fugacity from analyses of multicomponent iron-titanium oxides: *American Mineralogist*, 68(5-6), 586-594.
- Tuff, J., and O'Neill, H. S. C., 2010, The effect of sulfur on the partitioning of Ni and other first-row transition elements between olivine and silicate melt: *Geochimica et Cosmochimica Acta*, 74(21), 6180-6205, <https://doi.org/10.1016/j.gca.2010.08.014>
- Wood, B. J., and Virgo, D., 1989, Upper mantle oxidation state: Ferric iron contents of Iherzolite spinels by ^{57}Fe Mössbauer spectroscopy and resultant oxygen fugacities: *Geochimica et Cosmochimica Acta*, 53(6), 1277-1291, [https://doi.org/10.1016/0016-7037\(89\)90062-8](https://doi.org/10.1016/0016-7037(89)90062-8)
- Wood, B. J., Bryndzia, L. T., and Johnson, K. E., 1990, Mantle oxidation state and its relationship to tectonic environment and fluid speciation: *Science*, 248(4953), 337-345, <https://doi.org/10.1126/science.248.4953.337>.

Supplemental Figure Captions

Figure S1. A: SiO_2 vs. $(\text{K}_2\text{O}+\text{Na}_2\text{O})$ diagram of ultrapotassic volcanic rocks. B: SiO_2 vs. K_2O diagram. Data source is [Table S5](#). Abbreviations: UVR = ultrapotassic volcanic rock

Figure S2. Photomicrographs and Back-scattered-electron (BSE) images illustrating the petrographic characteristics of ultrapotassic volcanic rocks. A–C: Photomicrographs showing a gradually decreasing trend of the proportion of olivine phenocryst from the most mafic Sailipu trachyandesite to the most silicic Mibale trachyte. D–F: BSE images (D and F) and photomicrographs (E) illustrating an increasing trend of the proportion of magnetite from trachyandesite to trachyte, while the proportion of both ilmenite and sulfide decreases. G: BSE image showing olivine phenocryst of Sailipu trachyandesite which contains pentlandite, chalcopyrite, sanidine and phlogopite inclusions. H: BSE image showing chalcopyrite inclusion occurred in clinopyroxene of Chazi trachyandesite. I: Clinopyroxene phenocryst in Mibale trachyte contains ilmenite, sanidine and apatite inclusions. Abbreviations: Ap = apatite; Ccp = chalcopyrite; Cpx = clinopyroxene; Ilm = ilmenite; Mag = magnetite; Ol = olivine; Phl = phlogopite; Pn = pentlandite; San = sanidine; Sp = spinel; Zrn = zircon

Figure S3. Photomicrographs of mineral and melt inclusions, and Raman spectrum diagrams of gas bubbles coexisting with mineral and melt inclusions. A, C, and E: Plane-polarized light photomicrographs of apatite inclusions coexisting with gas bubble enclosed in clinopyroxene phenocrysts of ultrapotassic volcanic rocks. B, D, and F: Raman spectrum diagrams of gas bubbles coexisting with mineral inclusions in A, C, and E, respectively. G and I: Plane-polarized light photomicrographs of glassy melt inclusions coexisting with gas bubble enclosed in orthopyroxenes of lherzolite xenoliths. H and J: Raman spectrum diagrams of gas bubbles coexisting with melt inclusions in G and I, respectively. Abbreviations: Ap = apatite; Cpx = clinopyroxene; MI = melt inclusion; Opx = orthopyroxene

Figure S4. Fresh lherzolite xenoliths in trachyandesite.

Figure S5. BSE images illustrating the petrographic characteristics of lherzolite xenoliths. In A and B, clinopyroxene often shows embayed texture filled by orthopyroxene. C: Vermicular Cr-rich spinel mainly occurred in the core of olivine. Abbreviations: Ap = apatite; Cpx = clinopyroxene; Ol = olivine; Opx = orthopyroxene; Phl = phlogopite; Sp = spinel.

Figure S6. Plot of $\text{Cr}/(\text{Cr}+\text{Al})$ in Cr-rich spinels vs. $\text{Fe}^{3+}/\sum\text{Fe}_{\text{spinel}}$. Data source is [Table S1](#).

Figure S7. BSE images of olivine in lherzolite xenolith (A) and olivine phenocryst in host trachyandesite (B), showing concentrations (ppm) of Ba, K and Th. The \pm values represent analysis precision (ppm) of each element. Data source is [Table S6](#). Abbreviations are similar with Figure S5.

Figure S8. Ba/La vs. Th/Yb diagram (A), Fe_2O_3 vs. Ba/La (B) and Th/Yb (C) diagrams of the Gangdese lower crustal samples. Data source is [Table S7](#).

Table S1–S7 are available as separate Excel files:

Table S1. EMPA data of olivine–spinel pairs and calculated $f\text{O}_2$ results of lherzolite xenoliths.

Table S2. Calculated temperature and pressure results of ultrapotassic volcanic rocks and lherzolite xenoliths.

Table S3. Calculated $f\text{O}_2$ results of ultrapotassic volcanic rocks by the $D_{\text{V}}^{\text{ol/melt}}$ oxybarometer.

Table S4. Published Os and Sr isotope data of ultrapotassic volcanic rocks. Data are from Liu et al. (2014).

Table S5. Major and trace element, and Sr–Nd–Pb isotope data of ultrapotassic volcanic rocks. Published data are from Zhao et al. (2009) and Guo et al. (2013; 2015).

Table S6. The contents of highly incompatible elements in olivine analyzed by *in-situ* LA-ICP-MS.

Table S7. Published major and trace element data of the Mesozoic and Cenozoic lower crustal samples. Data are from Zhang et al. (2019).

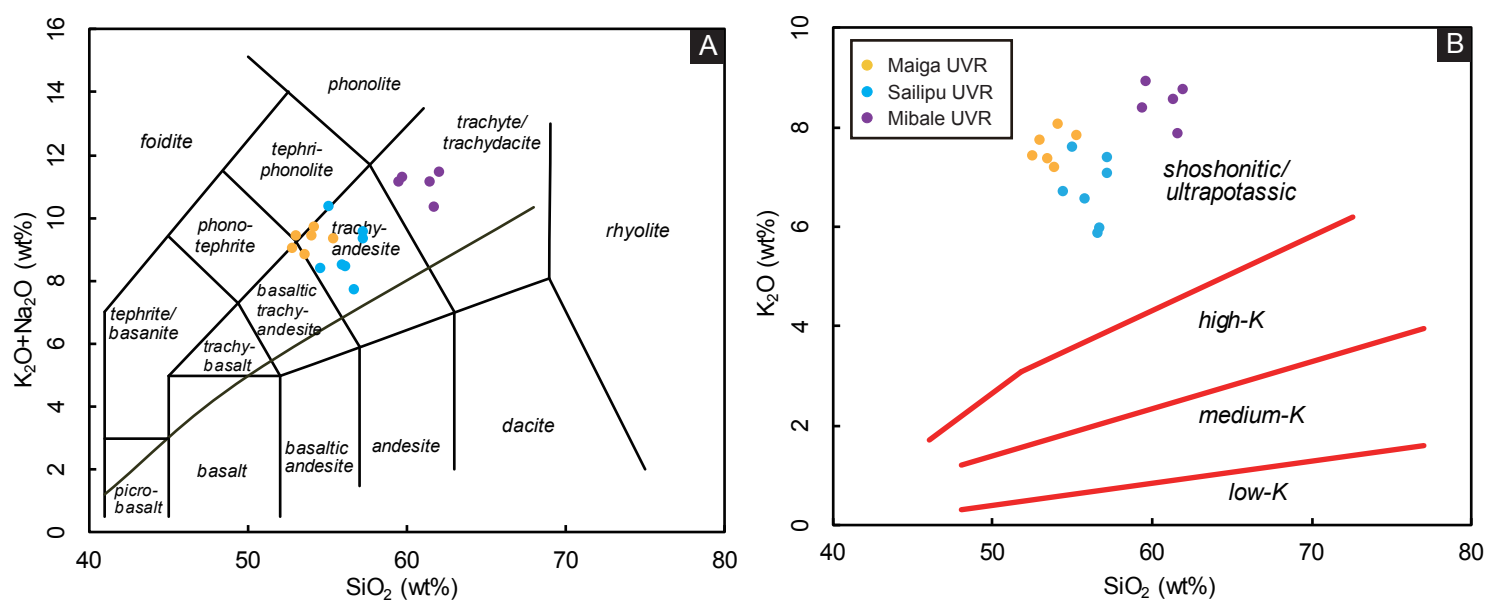


Fig. S1

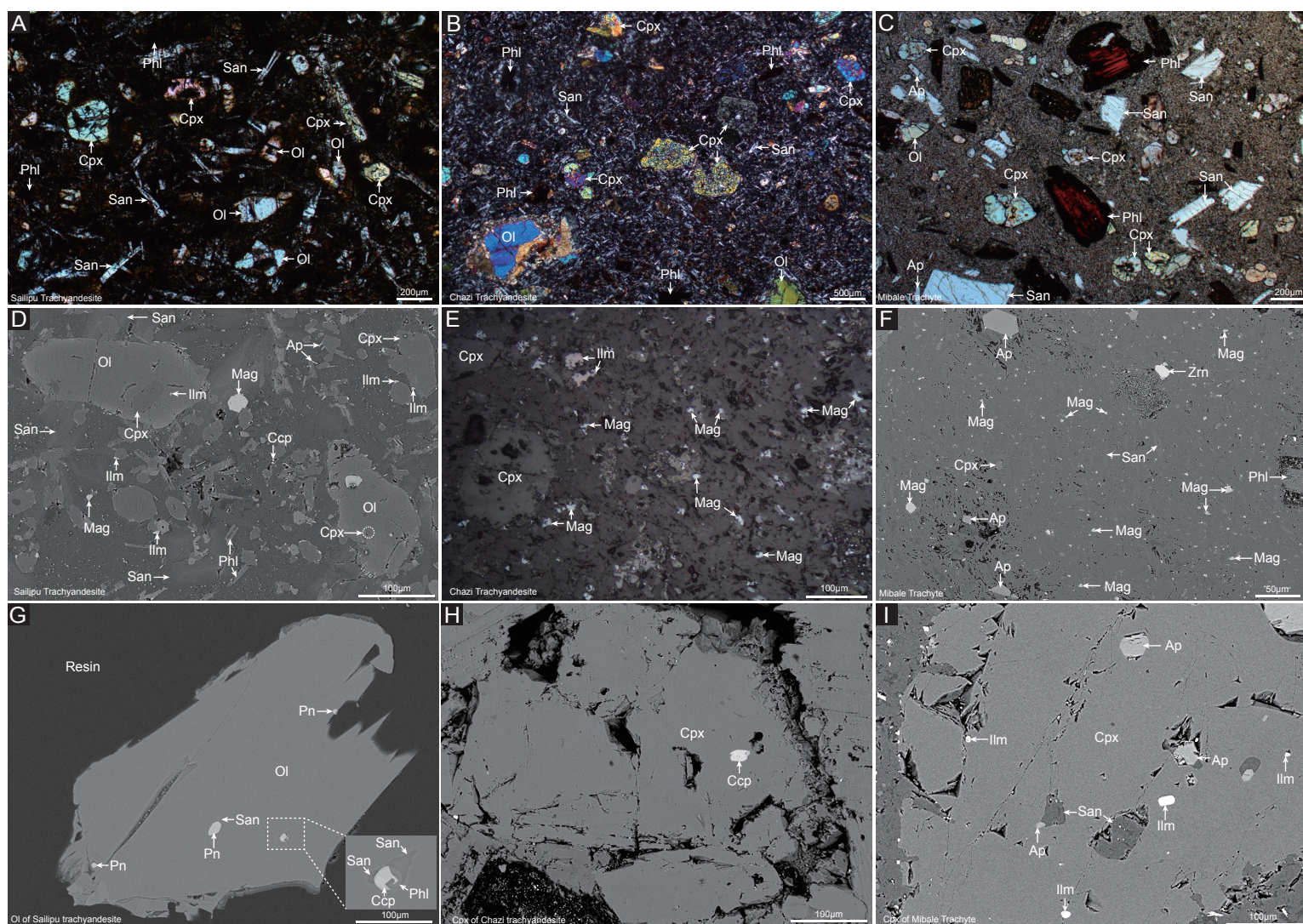


Fig. S2

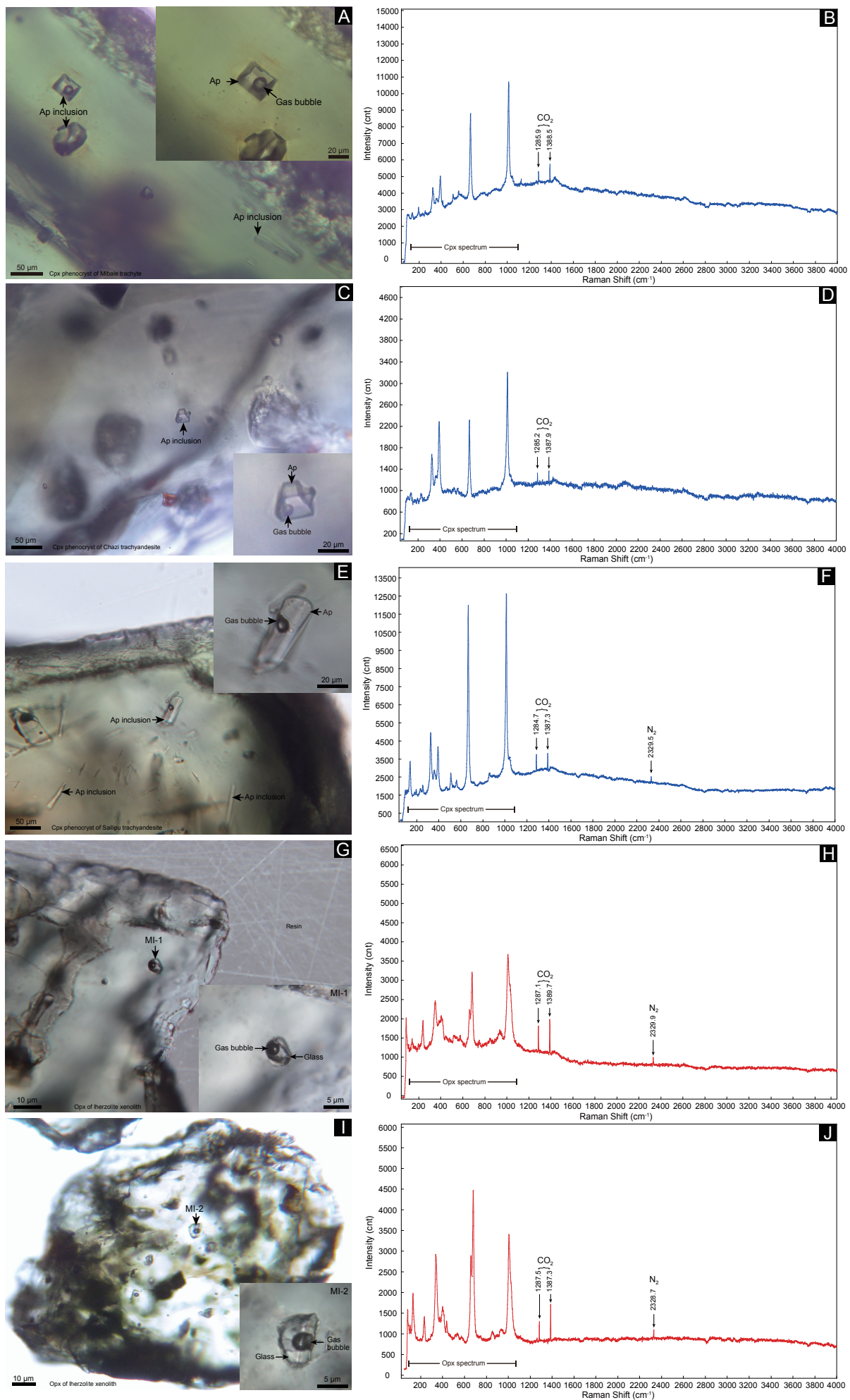


Fig. S3

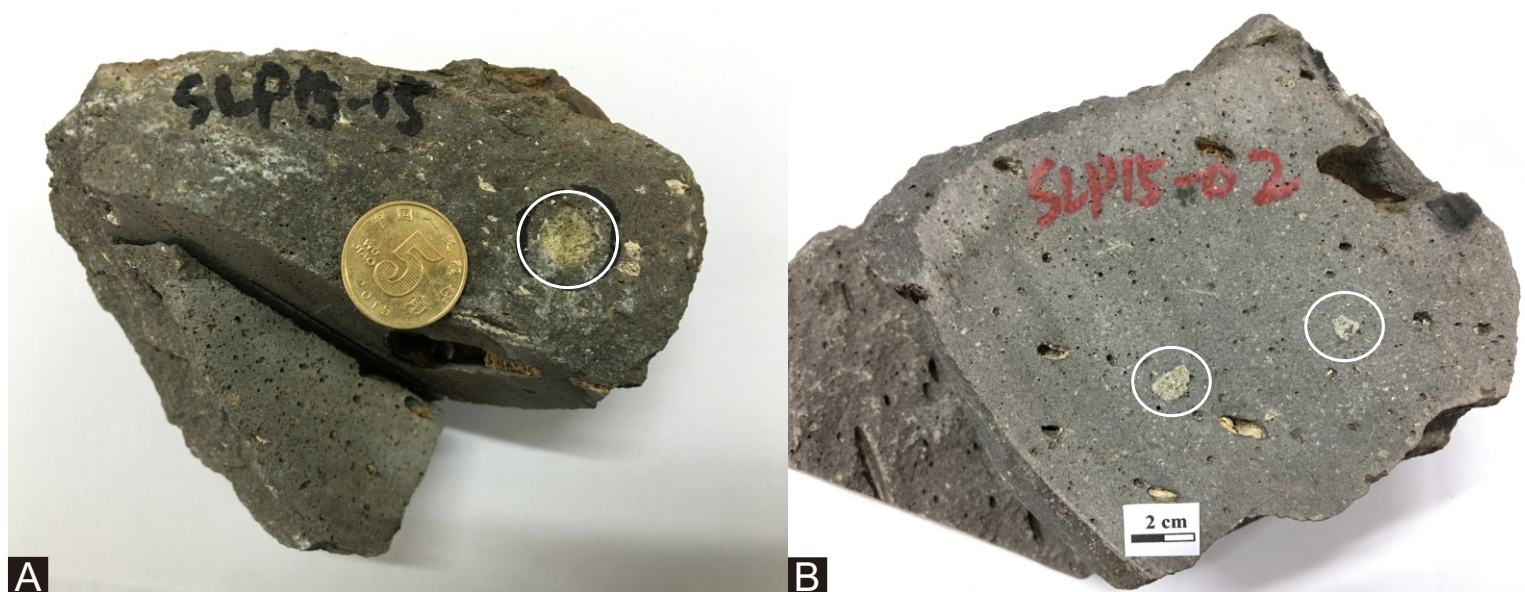


Fig. S4

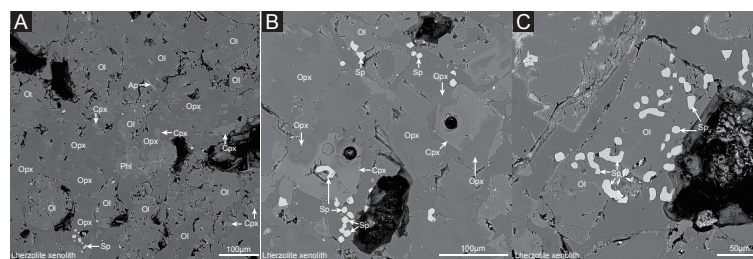


Fig. S5

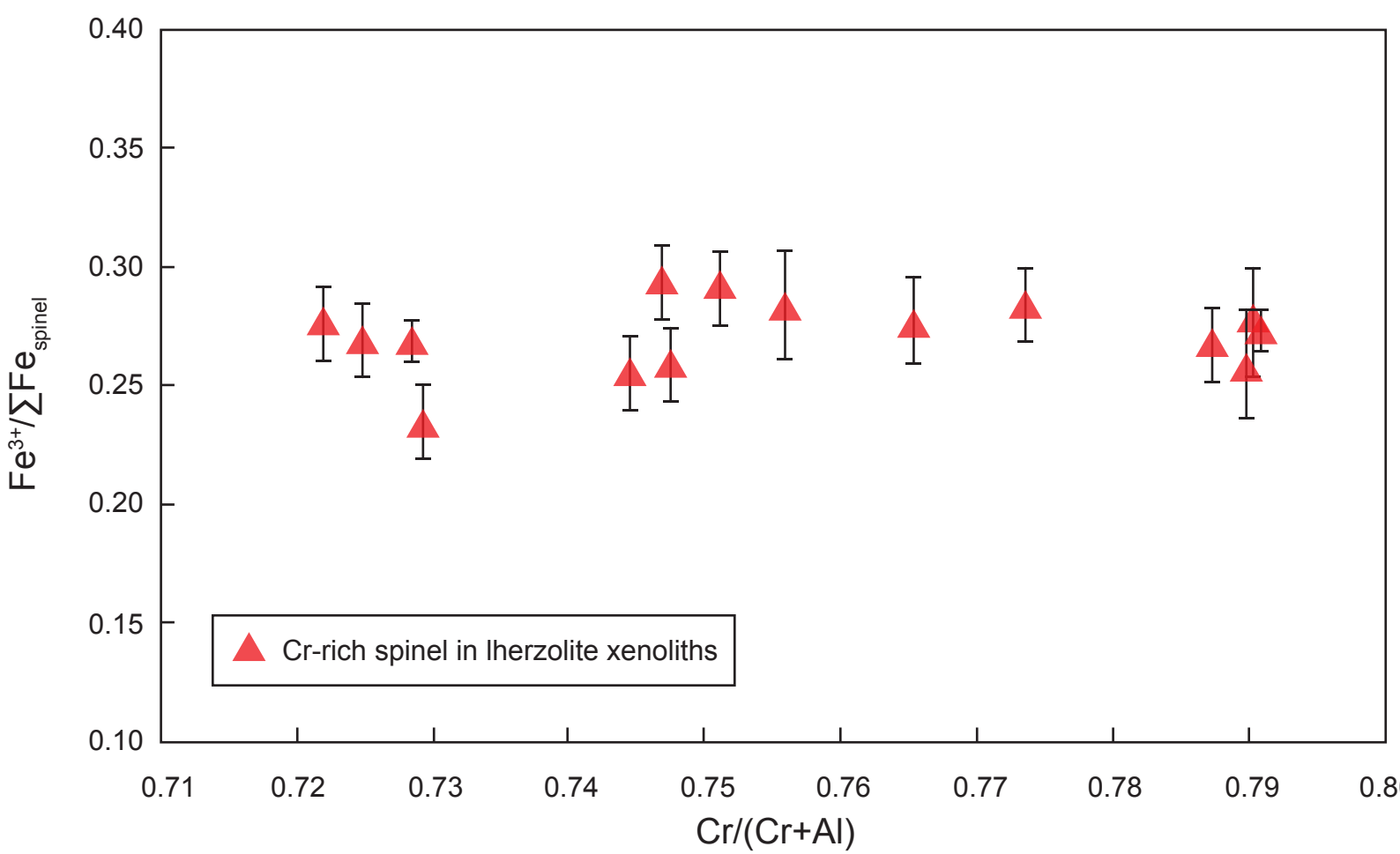


Fig. S6

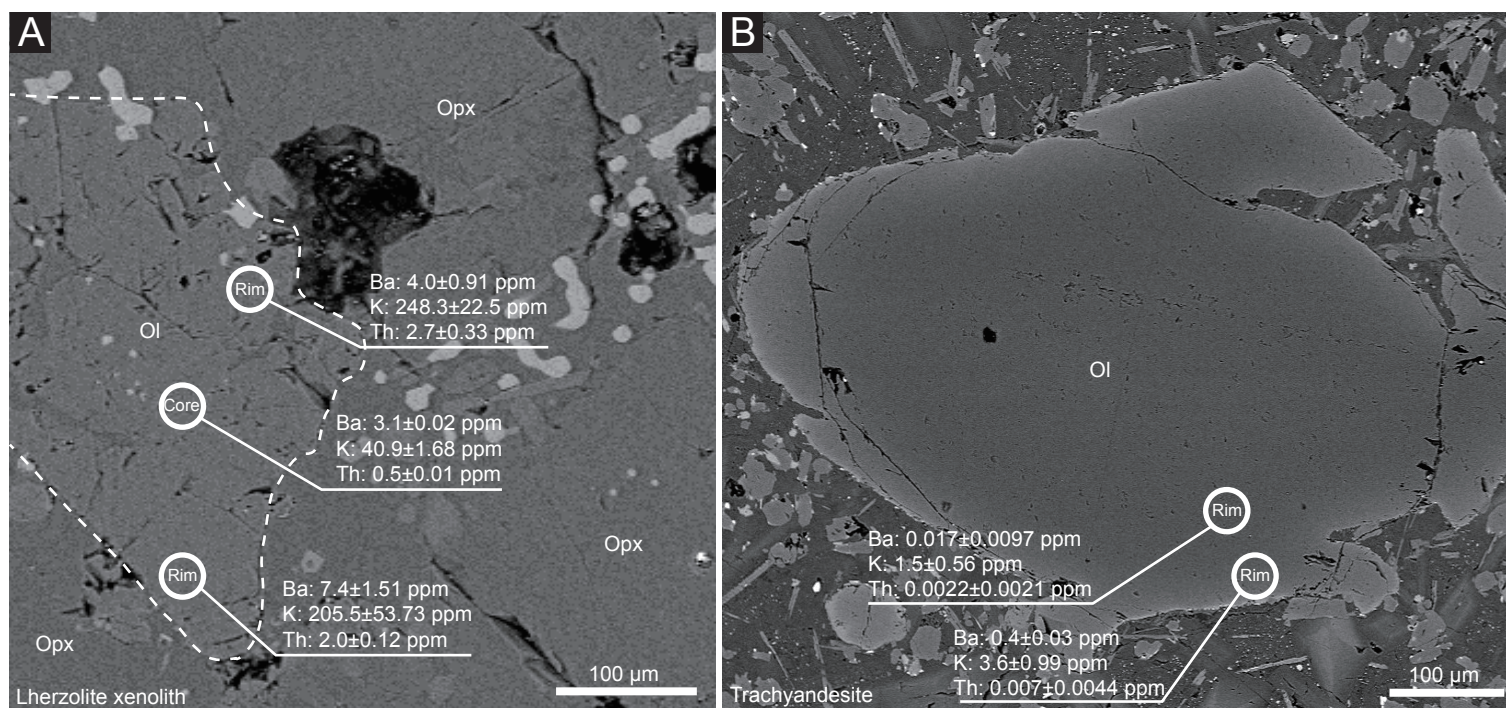


Fig. S7

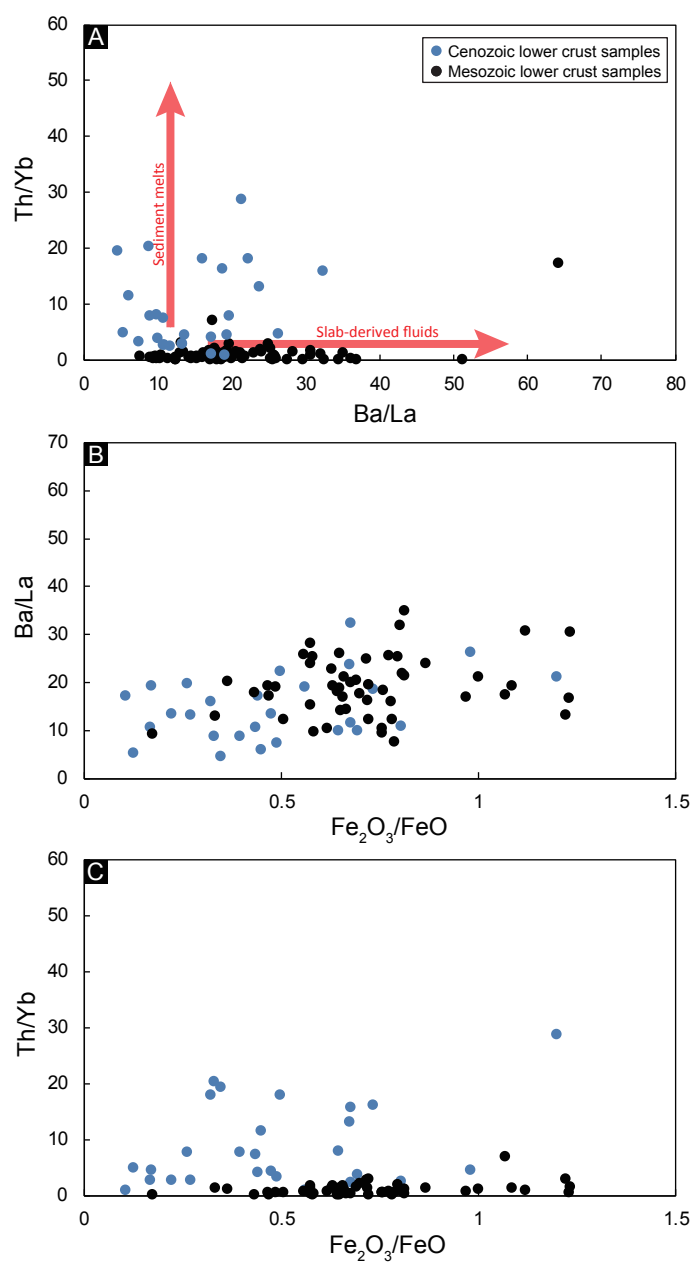


Fig. S8